Published OnlineFirst October 11, 2021; DOI: 10.1158/2326-6066.CIR-21-0493

Monitoring PD-1 Phosphorylation to Evaluate PD-1 Signaling during Antitumor Immune Responses

Xia Bu[1], Vikram R. Juneja[2,3,4], Carol G. Reynolds[1], Kathleen M. Mahoney[1], Melissa T. Bu[1], Kathleen A. McGuire[3,4], Seth Maleri[3,4], Ping Hua[1], Baogong Zhu[1], Sarah R. Klein[1], Edward A. Greenfield[1], Philippe Armand[1], Jerome Ritz[1], Arlene H. Sharpe[3,4], and Gordon J. Freeman[1]

ABSTRACT

PD-1 expression marks activated T cells susceptible to PD-1–mediated inhibition but not whether a PD-1–mediated signal is being delivered. Molecular predictors of response to PD-1 immune checkpoint blockade (ICB) are needed. We describe a monoclonal antibody (mAb) that detects PD-1 signaling through the detection of phosphorylation of the immunotyrosine switch motif (ITSM) in the intracellular tail of mouse and human PD-1 (phospho-PD-1). We showed PD-1$^+$ tumor-infiltrating lymphocytes (TILs) in MC38 murine tumors had high phosphorylated PD-1, particularly in PD-1$^+$TIM-3$^+$ TILs. Upon PD-1 blockade, PD-1 phosphorylation was decreased in CD8$^+$ TILs. Phospho-PD-1 increased in T cells from healthy human donors after PD-1 engagement and decreased in patients with Hodgkin lymphoma following ICB. These data demonstrate that phosphorylation of the ITSM motif of PD-1 marks dysfunctional T cells that may be rescued with PD-1 blockade. Detection of phospho-PD-1 in TILs is a potential biomarker for PD-1 immunotherapy responses.

Introduction

Antibodies blocking the programmed death (PD)-1 pathway have shown remarkable clinical efficacy across multiple cancers (1–3). However, only a subset of patients receiving these therapies have durable, objective responses. Data from a large volume of clinical research show a wide range of response rates to PD-1–based immunotherapy, ranging from a high of 87% in Hodgkin lymphoma to a low of 14% in gastroesophageal cancer, the lowest FDA approved indication. Response rates in pancreatic, microsatellite-stable colorectal, and glioblastoma are 5% or less (4–6). The reasons for these highly variable response rates are not well understood. Great efforts have been taken to discover biomarkers that can predict the efficacy of PD-1–based cancer immunotherapy. PD-L1 expression, tumor mutational burden, interferon-gamma (IFNγ) gene signature, and others have been explored as biomarkers but have not been proven as broadly or highly predictive. This situation highlights the need for more accurate biomarkers that can assess the efficacy of PD-1 immunotherapies before and during treatment, such that the most efficient and effective treatment plan can be adopted (7–9).

A major challenge in identifying additional biomarkers that can shed light on PD-1 immune checkpoint blockade (ICB) efficacy is the complexity of the PD-1 pathway. Effector T cells express PD-1 upon activation, as do B cells, NK cells, and some myeloid cells (10). In addition to its expression on many cell subsets, PD-1 can have varying effects within different cell types upon interaction with its ligands. In activated T cells, PD-1 ligation diminishes TCR and CD28 signaling, resulting in a hierarchy of attenuated effector T-cell responses (e.g., production of specific cytokines, cytotoxicity, proliferation; ref. 11). Likewise, PD-1 expression has been observed on NK cells and inhibits cytotoxic activity (12, 13). In contrast, PD-1 ligation on regulatory T cells (Treg), which can express PD-1 under resting conditions, may impact Treg homeostasis and decrease Treg suppressive activity (14, 15). Thus, PD-1 blockade may activate and expand tumor-infiltrating PD-1$^+$ Treg cells, as well as increase PD-1$^+$CD8$^+$ T-cell functions. Suppressive Tregs predominate in patients who develop hyperprogressive disease following PD-1 blockade. The ratio of PD-1$^+$CD8 T cells to PD-1$^+$ Treg at the outset of treatment has been suggested as a biomarker for clinical response to PD-1 blockade and potential for hyperprogression, but additional biomarkers are needed. PD-1 functionality in myeloid cells is less clear, but studies show that PD-1 blockade enhances phagocytosis (16). The PD-1 ligands, PD-L1 and PD-L2, are expressed on multiple cell types; PD-L1 is broadly expressed on hematopoietic and nonhematopoietic cells, whereas PD-L2 is generally restricted to expression on antigen-presenting cells (APC) and airway epithelia (17). Both ligands can be expressed by tumor cells, either alone or together (17). PD-1 ligand expression in the tumor microenvironment and in draining lymph nodes (dLN) can contribute to PD-1 engagement and immunoinhibitory activity. Due to the complex function of PD-1 on various cell subsets and the broad expression of its ligands, it has proved difficult to accurately determine where and when PD-1 pathway blockade alters T-cell function.

To more carefully assess the efficacy of PD-1 pathway blockade in a cell-specific manner, we sought to generate antibodies to assess PD-1 activity. PD-1, a 288-amino acid protein, has a single extracellular

[1]Department of Medical Oncology, Dana-Farber Cancer Institute, and Department of Medicine, Harvard Medical School, Boston, Massachusetts. [2]Harvard-MIT Division of Health Sciences and Technology, Cambridge, Massachusetts. [3]Department of Immunology, Blavatnik Institute, Harvard Medical School, Boston, Massachusetts. [4]Evergrande Center for Immunologic Diseases, Harvard Medical School and Brigham and Women's Hospital, Boston, Massachusetts.

Note: Supplementary data for this article are available at Cancer Immunology Research Online (http://cancerimmunolres.aacrjournals.org/).

X. Bu and V.R. Juneja contributed equally to and share first authorship of this article.

A.H. Sharpe and G.J. Freeman contributed equally to and share senior authorship of this article.

Corresponding Author: Gordon J. Freeman, Dana-Farber Cancer Institute, 450 Brookline Avenue, Boston, MA 02215. Phone: 617–632–4585; Fax: 617–632–5167; E-mail: gordon_freeman@dfci.harvard.edu

Cancer Immunol Res 2021;XX:XX–XX

doi: 10.1158/2326-6066.CIR-21-0493

Published OnlineFirst October 11, 2021; DOI: 10.1158/2326-6066.CIR-21-0493

IgV-like domain and a 94-amino acid intracellular tail containing both an immunoreceptor tyrosine-based inhibitory motif (ITIM) and an immunoreceptor tyrosine-based switch motif (ITSM; ref. 18). Mutation of the Y223 in the ITIM motif has little effect on PD-1 immunoinhibitory function. However, mutation of tyrosine 248 in the ITSM motif (Y248) renders PD-1 non-functional *in vitro*, demonstrating that this residue is critical for PD-1 signaling (19, 20). Phosphorylation of Y248 leads to association of PD-1 with the T-cell receptor (TCR) in microclusters (21) and recruitment of SHP-2 (*Src* homology region 2 domain-containing phosphatase-2) to the cytoplasmic tail of PD-1, resulting in dephosphorylation of proximal signaling molecules downstream of CD28 and the TCR (22–26).

In this study, we developed a monoclonal antibody (mAb) that specifically recognizes phosphorylation of Y248 in the ITSM of PD-1. Our main goal was to establish a tool for studying active PD-1 signaling and to evaluate its use as a biomarker of successful PD-1 blockade. Current tools for assessing PD-1 signaling are limited. Because PD-1 is rapidly upregulated on T cells within hours of activation, PD-1 expression may indicate either an activated, functional T cell (no PD-1 ligation) or a suppressed T cell (PD-1 ligation). Thus, there is a need for a less ambiguous PD-1 associated marker for T-cell functionality. We reasoned that the detection of phosphorylated PD-1 could be used as a predictive biomarker to assess the response to PD-1 immunotherapy. We demonstrate that tumor-infiltrating lymphocytes (TIL) expressing multiple coinhibitory receptors, which have been shown to be more dysfunctional (27, 28), have higher phospho-PD-1. We also showed that tumor immunotherapy with PD-1 mAb resulted in reduced PD-1 phosphorylation in both mice and humans. Thus, this mAb has potential as a tool for both understanding the basic biology of the PD-1 pathway, as well as assessing clinical responsiveness to PD-1 and PD-L1 immunotherapies.

Materials and Methods

Cell lines

MC38 adenocarcinoma (a gift from D. Vignali of the University of Pittsburgh School of Medicine) and BRAF.PTEN melanoma tumor cells (29) were cultured in DMEM supplemented with 10% FBS (Thermo Fisher Scientific). Both cell lines were confirmed to be free of pathogens by MAP testing and of murine origin by flow cytometry, but not further verified. 4T1 (CRL-2539) mouse breast tumor, EL4 (TIB-39) mouse T-cell lymphoma, and Jurkat E6–1 (TIB-152) human T-cell lymphoma cells were purchased from ATCC and maintained in R10 media composed of RPMI1640 (Gibco 11875–093) supplemented with 10% FBS (Sigma Aldrich), 1% glutamax (Gibco 35050–061), 100 unit/mL penicillin and 100 μg/mL streptomycin (Gibco 15140–122), 15 μg/mL gentamacin (Gibco 15710–072). 300.19 mouse pre-B leukemia cells were obtained from Naomi Rosenberg of Tufts University School of Medicine and maintained in R10 plus 50 μmol/L 2-mercaptoethanol (Sigma Aldrich). 300-mouse (m)PD-1 and Jurkat-human (h)PD-1 stable cell lines were previously established in the lab (30, 31). 300-mPD-1 cells were maintained in R10 supplemented with 50 μmol/L 2-mercaptoethanol and 5 μg/mL puromycin (Invivogen). Jurkat-hPD-1 cells were maintained in R10 supplemented with 5 μg/mL blasticidin (Invivogen). SP2/0 myeloma cells (CRL-8006) were purchased from ATCC and maintained in DMEM media (Thermo Fisher Scientific) supplemented with 10% FBS. MRC-5 feeder cells (CCL-171) were purchased from ATCC and maintained in MEM media (Thermo Fisher Scientific) supplemented with 10% FBS. CHO-K1 cells (CCL-61) were purchased from ATCC and maintained in F12K media (Thermo Fisher Scientific) supplemented with 10% FBS. Caki-2 (HTB-47), human clear cell carcinoma cell line was purchased from ATCC and maintained in McCoy's 5a medium modified supplemented with 10% FBS. All ATCC-derived cell lines were cultured for fewer than 25 passages and were not reauthenticated upon receipt from ATCC. All cell lines and stably transfected cell lines were tested negative for *Mycoplasma* using the MycoAlert Mycoplasmid Detection Kit (Lonza LT07–118) or Venor GeM Mycoplasma Detection Kit (Sigma-Aldrich, MP0025).

Mice

Mice 6 to 10 weeks of age were used for all experiments. Wild-type (WT) C57BL/6 mice and *TCRα*$^{-/-}$ mice were purchased from the Jackson Laboratory. P14 TCR transgenic (Tg) were purchased from Jackson Lab and *Pdcd1*$^{-/-}$ mice (developed in Dr. Arlene Sharpe's lab) have been previously described (32, 33). All experimental mice were housed in specific pathogen–free conditions and used in accordance with animal care guidelines from the Harvard Medical School Standing Committee on Animals, Dana-Farber Cancer Institute, and the NIH. Animal protocols were approved by the Harvard Medical School Standing Committee on Animals.

Generation of phospho-PD-1 antibody

One hundred micrograms of human PD-1 p248Tyr peptide (CKK-aminocaproic acid-VPEQTE[pY]ATIVF-amide; synthesized at 21st Century Biochemical) conjugated to Keyhole limpet hemocyanin (KLH) protein (Sigma Aldrich) was suspended in PBS and emulsified in complete Freund's adjuvant (Sigma Aldrich). Female BALB/c *Pdcd1*$^{-/-}$ mice (32) were immunized by injection of the emulsion at three subcutaneous sites (under front legs with axial direction and base of tail) and one intraperitoneal site on day 0. Mice were boosted in incomplete Freund's adjuvant (Sigma Aldrich) on day 14 [100 μg PD-1 p248Tyr peptide conjugated to ovalbumin (OVA) protein (Sigma Aldrich), s.c.], day 28 (100 μg PD-1 p248Tyr peptide conjugated to KLH protein, s.c.), and day 56 (50 μg PD-1 p248Tyr peptide conjugated to KLH protein in PBS, i.v.). On day 60, mice were euthanized, their spleens were removed and made into a single cell suspension by mashing the spleen in a petri dish with the back of a 5 mL syringe plunger (Becton Dickinson), then the cells passed through a 70 μm cell strainer (Falcon) using 10 mL DMEM media. The single-cell suspensions from the spleen were mixed with SP2/0 myeloma cells at a splenocyte to myeloma ratio of 2:1. Cells were fused with polyethylene glycol 1450 (ATCC; ref. 34) in twelve 96-well tissue culture plates in HAT selection medium composed of 80 mL DMEM (Cellgro, 15–017-CM), 75 mL Fetal Bovine Serum (Hyclone, SH30070.03), 3.9 mL Glutamax (GIBCO, 35030), 3.9 mL NCTC-109 (GIBCO, 21340), 3.9 mL Penicillin/Streptomycin (GIBCO, 15140), 0.3 mL Gentamycin (Sigma Aldrich, G1397), 4 mL HAT supplement (ATCC, 69-X), 9 mL Hybridoma Cloning Supplement (PAA Laboratories, P05–009). The HAT supplement was replaced with HT supplement (ATCC, 71-X) at 7 days after fusion. Hybridoma wells were screened by ELISA (as described below) for reactivity with the PD-1 p248Tyr peptide conjugated to BSA and lack of reactivity to unphosphorylated PD-1 peptide conjugated to BSA or to BSA and by Western blot on pervanadate-treated Jurkat-hPD-1 lysates (as described below). Clone 407.6G12 (mouse IgG2a, kappa) was selected, subcloned, and purified mAb prepared as described below.

Clone selection, cloning, and purification

Cloning

Fifty microliters of medium supplemented with 20% FBS (Sigma) and 3% to 5% Hybridoma Cloning Factor (Antibody Research, Inc.)

Published OnlineFirst October 11, 2021; DOI: 10.1158/2326-6066.CIR-21-0493

was added to each well of a 96-well plate (Corning) containing 50 μL of MRC-5 feeder cells (ATCC CCL-171), giving a total volume of 100 μL/well. 100 μL of the hybridoma cell suspension was removed and transferred to the top left-hand well and mixed by pipetting. 1-in-2 dilutions were performed down the left-hand row of the plate (eight wells; seven dilution steps), followed by 1-in-2 dilutions across the plate using a multichannel pipette. Clones are visualized by microscopy after 10 to 12 days. Single-cell wells were selected for expansion.

Antibody purification

The selected hybridoma was grown in four T175 flasks (Corning) in D10 medium (about 1 liter) composed of 180 mL DMEM (Cellgro, 15–017-CM), 75 mL fetal bovine serum (Hyclone, SH30070.03), 3.9 mL Glutamax (GIBCO, 35030), 3.9 mL penicillin/streptomycin (GIBCO, 15140), 0.3 mL gentamycin (Sigma Aldrich, G1397), and 9 mL Hybridoma Cloning Supplement (PAA Laboratories, P05–009), until the cultures were exhausted. Cells were centrifuged, and antibody-rich medium was purified using an AKTA Express (GE Healthcare) fitted with a protein A column (GE Healthcare). The antibody was eluted with low pH glycine/HCl buffer, pH 2.6 buffer directly into tubes containing 1 M Tris/HCl pH 9.0, combined, dialyzed against PBS (Sigma) overnight, and concentrated to 1 mg/mL using Centricons (Amican).

ELISAs

High-protein binding 96-well EIA plates (Costar/Corning) were coated with 50 μL/well of a 2 μg/mL solution (0.1 μg/well) of PD-1 p248Tyr peptide conjugated to BSA (Sigma) or an irrelevant peptide conjugated to BSA and incubated overnight at 4°C. Excess solution was aspirated, and the plates were washed three times with PBS/0.05% Tween-20, then blocked with 1% bovine serum albumin (BSA, fraction V, Sigma Aldrich) for 1 hour at room temperature to prevent nonspecific binding. The BSA solution was removed, and 50 μL/well of hybridoma supernatant from each fusion plate well was added. The plates were then incubated for 45 minutes at 37°C and washed three times with PBS/0.05% Tween-20. Horseradish peroxidase (HRP)–conjugated $F(ab')_2$ goat anti-mouse IgG (H+L; Jackson Immunoresearch Laboratories) diluted 1:4000 in 1% BSA/PBS was added to each well, and the plates were incubated for 45 minutes at 37°C. Plates were washed three times with PBS/0.05% Tween-20, and 50 μL/well of ABTS solution (Zymed) was added. The intensity of the green color of positive wells was read on a Spectramax microtitre plate reader at 405 nm wavelength (Molecular Devices Corp). Supernatant from the SP 2/0 myeloma cells was used as a negative control, and immune sera from the mouse that was used for the fusion was diluted 1:5000 as the positive control.

Western blot

Jurkat hPD-1 or EL4 (10×10^6 cells) were treated for 5 minutes at 37°C with 0.1 mmol/L pervanadate (premixing orthovanadate, Na_3VO_4 (Sigma Aldrich) and H_2O_2 (Sigma Aldrich) for 15 minutes at room temperature to generate pervanadate), and cells were lysed in RIPA buffer (Boston Bioproducts) supplemented with Protease Inhibitor Cocktail (Roche; one tablet in 10 mL of RIPA buffer) and lysates were prepared (36–39). Cell lysates (20 μg) were separated on 4% to 15% Mini-Protean TGX gels (Bio-Rad) and transferred onto nitrocellulose blotting membranes (Amersham). A blocking buffer of 5% milk (Fisher) in 1XTBS-T (1X TBS + 0.1% Tween-20) was used to block nonspecific binding by incubation for 1 hour at room temperature. Primary antibodies against phospho-PD-1 (clone 407.6G12), anti-mouse PD-1 (clone 29F.1A12; ref. 35), or anti-human PD-1 (clone EH33; ref. 40) diluted to 2 μg/mL in 1% BSA in TBS-T were incubated with the membrane overnight at 4°C. After washing three times with TBS-T, the membrane was incubated with HRP-conjugated goat anti-mouse IgG or anti-rat IgG secondary antibody (Southern Biotech) diluted 1:5000 in 2.5% milk in TBS-T buffer plus 1% normal goat serum (Southern Biotech) for 1 hour at room temperature. Immunoreactive proteins were detected using enhanced chemiluminescence reagent ECL (PerkinElmer; ref. 41).

Generation of a PD-L1 tetramer

A mPD-L1 kappa/mPD-L1-hIgG1 fusion protein tetramer was generated using the In-fusion cloning method (42). The extracellular domain of mPD-L1 (accession number NM_021893) with a 17-amino acid linker (GGSGGTGGSGGTGGSGG) was linked separately to human Kappa constant region (accession number JQ837832.1) or IgG1 CH1-hinge-CH2CH3 region (accession number BC075842.1) in the pEFGF expression vector (43). and expressed in CHO cells (43). The Fc fusion protein was produced and purified from CHO cell culture supernatants by protein G affinity chromatography and verified to have endotoxin levels less than 2 EU/mg protein (contract service by BioXCell).

PD-L1 tetramer treatment and IL2 ELISAs

1×10^5 Jurkat hPD-1 cells/well were cultured in 96-well round-bottom plates with the PD-L1 tetramer (15 μg/mL) for 1 hour, then treated with anti-human CD3 (0.1 μg/mL Fitzgerald, clone T3/4E) and anti-human CD28 (0.3 μg/mL, Fitzgerald, clone 15E8) for 24 hours. Cell culture supernatants were harvested and assayed undiluted for IL2 using the Duoset human IL-2 ELISA kit (R&D) according to the manufacturer's protocol. A standard curve was constructed with the provided IL2 standard. Media alone was used as a negative control.

Patients

We obtained peripheral blood samples from 3 patients with classical Hodgkin lymphoma who were enrolled in a clinical trial combining anti–PD-1 (nivolumab) with the investigational anti–LAG-3 relatlimab (NCT02061761). The inclusion criteria for the present analysis included a documented diagnosis of classical Hodgkin lymphoma, receipt of an anti–PD-1 mAb, and availability of pre- and post-treatment peripheral blood samples. There were no exclusion criteria. Patients provided written informed consent for the banking and research use of samples through an IRB-approved institutional banking protocol. The clinical trial was conducted in accordance with the principles of the Declaration of Helsinki. The peripheral blood samples were collected from the patients before treatment on the first day of treatment and at 15 days, 15 days, or 21 days (respectively, for the 3 patients) after the first treatments with one dose of nivolumab (240 mg) and relatlimab (160 mg) combination therapy (intravenous infusion). Peripheral blood mononuclear cells (PBMC) were processed and stored in liquid nitrogen at the Pasquarello Tissue Bank of Dana-Farber Cancer Institute. Samples were thawed and analyzed by flow cytometry as described below.

Tumor studies

WT or *Pdcd1*$^{-/-}$ C57BL6/J mice were injected subcutaneously in the right flank with 1×10^5 MC38 or BRAF.PTEN tumor cells. Mice were sacrificed when tumor size reached experimental endpoint (tumor >2 cm diameter or upon tumor >1.0 cm with tumor ulceration >0.5 cm diameter). Where indicated, mice were given 200 μg anti–PD-1 (clone 29F.1A12; BioXCell) or isotype control antibody rat IgG2a

Published OnlineFirst October 11, 2021; DOI: 10.1158/2326-6066.CIR-21-0493

(clone 2A3; BioXCell) intraperitoneally at days 7, 10, and 13 after tumor implantation. Tumors were measured by caliper every 2 to 3 days until they reached the experimental endpoint or until the time point listed for analysis (days 7, 10, and 20).

TIL isolation

Tumors and dLNs were harvested, dissected, mechanically disaggregated to about 2 to 3 mm pieces, and digested with collagenase type I (400 U/mL; Worthington Biochemical) and 200 U/mL DNase I (Roche) for 30 minutes on an end-over-end rotator at 37°C. Following digestion, the cells were passed through 70 μm cell strainers (Fisher), centrifuged at 350 rcf for 5 minutes, and the supernatant aspirated. Cells were resuspended in 2 mL RBC (red blood cell) lysis buffer (Sigma Aldrich), gently mixed, and incubated on ice for 2 minutes. Cells were washed once with MACS buffer (Hank's Balanced Salt Solution without $Ca2^+$, without $Mg2^+$ (Gibco), 1% FBS, 2 mmol/L EDTA) by centrifuging at 350 rcf for 5 minutes. Cells were layered on a Percoll (GE Healthcare) gradient (40% and 70%) and centrifuged at 375 rcf, 30 minutes at room temperature (no brake), and the layer of mononuclear cells was harvested. Cells were washed in MACS buffer, resuspended in MACS buffer, and analyzed by flow cytometry as described below.

In vitro T-cell stimulation

$CD8^+$ T cells from the spleens of P14 *TCR* Tg mice were isolated using a $CD8\alpha^+$ T-cell isolation kit for positive selection (Miltenyi Biotec), which led to purities >99%. 5×10^4 $CD8^+$ T cells were plated on 1×10^5 irradiated splenocytes from $TCR\alpha^{-/-}$ mice (3000 rads using a gamma irradiator, JL Shepherd and Associates, Model Mark 1, source isotope is Cesium-137). One microgram of GP33–41 peptide (Genscript) was added, and cells were incubated at 37°C for 72 hours prior to analysis. Following written consent to use the blood, human PBMCs were prepared from six healthy donors by Ficoll-Paque plus (GE Healthcare) gradient centrifugation. $CD3^+$ T cells were isolated using the human Pan T-cell Isolation Kit (Miltenyi) and cultured in 24-well plates (1×10^6 cells in 1 mL R10 media with or without anti-CD3 (0.1 μg/mL, Fitzgerald, clone T3/4E) and anti-CD28 (0.3 μg/mL, Fitzgerald, clone 15E8) stimulation for 24 hours. Cells were further incubated with or without the indicated concentration of PD-L1 tetramer for another 24 hours.

Flow cytometric analysis of T cells

Cells cultured *in vitro* (human and mouse) or isolated from the tumors or dLNs of mice were stained with the following directly labeled antibodies to surface molecules (all from Biolegend). Human panel: Live/Dead Yellow, CD3 Brilliant Violet 605 (UCHT1), CD4 FITC (RPA-T4), CD8 PE-Cy7 (HIT8a), PD-1 PE (EH12); mouse panel: Live/Dead near IR, anti-mCD45.2 (104), anti-mCD3e (145–2c11), anti-mCD4 (RM4–5), anti-mCD8a (53–6.7), anti-mPD-1 (RMP1–30), and anti-mTIM-3 (RMT3–23).

Mouse sample staining

One microgram of anti-CD16/32 (clone 2.4G2, BioXCell) per 100 μL was first added to mouse cells to block Fc receptors. Staining was performed for 30 minutes on ice, protected from light. After staining, cells were fixed and permeabilized using an Intracellular Fixation Buffer (eBioscience #88–8824–00) for 30 minutes on ice and then stained with phospho-PD-1 mAb Brilliant Violet 421 (10 μg/mL; clone 407.6G12, custom conjugated by Biolegend) on ice for 30 minutes. Isotype control and Fluorescence Minus One control were used for gating. Samples were analyzed on an LSR II or a FACSCanto II HTS (BD Biosciences) and analyzed using FlowJo software (TreeStar). A sample gating strategy can be found in Supplementary Fig. S1A.

Patient sample staining

Frozen PBMCs were thawed, 2.5 μg of human BD Fc block (BD Biosciences, 564219) per 100 μL was first added to human cells to block Fc receptors, and stained with CD3 BV786 (clone UCHT10), CD4 APC/Cy7 (clone SK3), CD8 pacific orange (clone SK1), CD45 RO FITC (clone UCHL1), CCR7 PE/Cy7 (clone G043H7; all from BioLegend) at 4°C for 20 minutes and washed twice with FACS buffer (PBS+2%FBS + 0.1 mmol/L EDTA). Cells were fixed and permeabilized with IC Fixation Buffer and Permeabilization Buffer (eBioscience #88–8824–00) and stained with phospho-PD-1 mAb conjugated with BV421 (10 μg/mL; clone 407.6G12) or mouse IgG2a BV421 antibody (BioLegend) for 30 minutes at room temperature, washed twice with permeabilization buffer, and analyzed by flow cytometry on a BD Canto cytometer. Note that the phospho-PD-1 mAb worked in conjunction with this permeabilization buffer but not the harsher buffer used for FoxP3 intranuclear staining. The data was analyzed using FlowJo software (TreeStar). A sample gating strategy can be found in Supplementary Fig. S1B.

Statistics

All statistical analysis was performed with Prism software 9.2.0 (GraphPad) and statistical significance determined where the *P* value was less than 0.05 (*), 0.01 (**), 0.001 (***), 0.0001 (****), or not significant (ns) when the *P* value was more than 0.05. Standard deviation (SD) is shown in the graphs. A two-tailed paired *t* test was used for comparison of two groups with paired samples. A two-tailed unpaired *t* test was used for comparison of two unpaired groups. A one-way ANOVA was used for single comparisons with more than two groups.

Results

mAb to detect phosphorylation of the ITSM motif of PD-1

The tyrosine 248 (Y248) of the ITSM of the PD-1 intracellular tail is critical for PD-1 signaling (19). We immunized $Pdcd1^{-/-}$ mice with a phosphorylated peptide immunogen encompassing the ITSM with a phosphorylated Y248 residue, which also included an eight amino acid sequence identical in mouse and human PD-1 (**Fig. 1A**). Following hybridoma fusion, we screened for mAbs that bound to the phospho-peptide but lacked reactivity with unphosphorylated peptide or carrier (see "Materials and Methods"). To further test these mAbs, we analyzed protein extracts from $PD\text{-}1^+$ and $PD\text{-}1^-$ human and mouse T-cell lines treated with pervanadate, a protein tyrosine phosphatase inhibitor known to stabilize the phosphorylation of proteins. One mAb clone (407.6G12) detected a band only in pervanadate-treated, $PD\text{-}1^+$ samples, and this band corresponded in size to PD-1. We confirmed PD-1 protein expression in all relevant samples (**Fig. 1B**). These results show that the 6G12 mAb clone detects phosphorylated Y248 PD-1.

To further examine the utility of this mAb, we tested its ability to detect phosphorylation of PD-1 by flow cytometry. We used Jurkat cells, a human T-cell line, stably transfected with human PD-1 (Jurkat-hPD-1). We detected low phospho-PD-1 in untreated Jurkat-hPD-1 cells compared to an isotype control. Phospho-PD-1 increased following pervanadate treatment (**Fig. 1C**). These results show that mAb 407.6G12 (hereafter referred to as

Published OnlineFirst October 11, 2021; DOI: 10.1158/2326-6066.CIR-21-0493

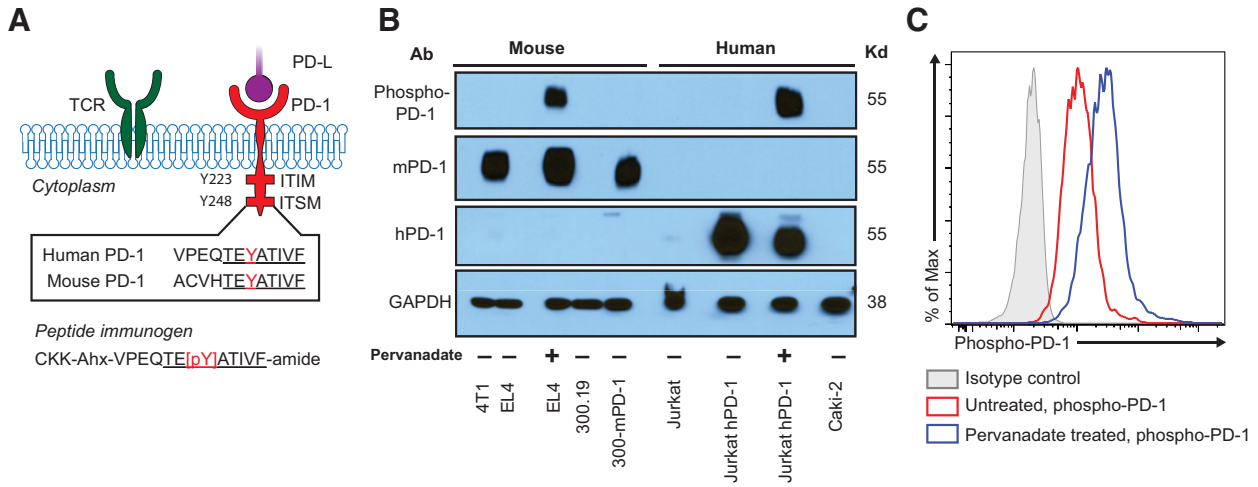

Figure 1.

Development of the phospho-PD-1 antibody. **A,** Phospho-peptide immunogen containing the conserved amino acid sequence encompassing the ITSM motif of the mouse and human PD-1 cytoplasmic tail. The red Y indicates the tyrosine in the ITSM that can be phosphorylated. **B,** Lysates were made from the indicated cell lines and Western blotted. EL4 and 300-mPD-1 cells were used as positive controls for mPD-1 cells, and Jurkat hPD-1 cells were used as positive controls for hPD-1 cells. Pervanadate-treated EL4 and Jurkat-hPD-1 were used to assess PD-1 phosphorylation. 4T1 and 300.19 were used as negative controls for mouse lysates, and Jurkat and Caki-2 cells were used as negative controls for human lysates. Samples were blotted with antibodies against phospho-PD-1 (6G12), mPD-1 (29F.1A12), hPD-1 (EH33), and GAPDH (loading control). **C,** Phospho-PD-1 expression in Jurkat-hPD-1 cells without treatment (red) or treated with pervanadate (blue). Data representative of three independent experiments.

"phospho-PD-1 mAb") can detect the phosphorylated form of the PD-1 ITSM by both Western blot and flow cytometry.

Ligation of PD-1 by PD-L1 leads to PD-1 phosphorylation and inhibition of IL2

We next tested whether the phospho-PD-1 mAb could detect PD-1 phosphorylation following PD-1 ligation by PD-L1. Current soluble recombinant reagents for ligating PD-1 have limited strength of signal. To overcome this limitation, we developed a tetramer in which a molecule of PD-L1 was linked to each of the IgG1 heavy and kappa chains, resulting in four molecules of PD-L1 on an antibody structure (**Fig. 2A**; referred to as PD-L1 tetramer). We hypothesized that this approach would allow for stronger ligation and cross-linking of PD-1 by PD-L1. To test this, we utilized the Jurkat-hPD-1 cell line, which expresses high human (h)PD-1 (**Fig. 2B**). We stimulated Jurkat-hPD-1 cells for 24 hours with anti-CD3/CD28 and PD-L1 tetramer or control antibody. Because PD-1 signaling is known to reduce IL2 production (19, 25), we measured IL2 in culture supernatants to confirm PD-1 signaling (**Fig. 2C**). The PD-L1 tetramer suppressed IL2 production in a dose-dependent fashion. Maximal inhibition of IL2 production was reached by 10 μg/mL, which was used for subsequent studies (**Fig. 2C**). We then used the PD-L1 tetramer to ligate PD-1 on Jurkat-hPD-1 cells and tested the ability of the phospho-PD-1 mAb to detect PD-1 phosphorylation by flow cytometry. Treatment with the PD-L1 tetramer led to an increase in phospho-PD-1 signal compared to baseline without PD-L1 tetramer treatment (**Fig. 2D**). This natural phospho-PD-1 signal was detectable by flow cytometry within 10 minutes, increased at 1 hour, and was seen in all cells at 2 hours post PD-1 ligation by PD-L1 tetramer (**Fig. 2E**). Together, these data indicate that the phospho-PD-1 mAb can be used to detect active PD-1 signaling induced by PD-L1 ligation.

We next tested whether the phospho-PD-1 mAb could detect a phospho-PD-1 signal induced by PD-L1 signaling from APCs. We compared WT and control PD-1 deficient (*Pdcd1*$^{-/-}$) CD8$^+$ T cells from P14 TCR transgenic mice, in which all T cells have a TCR that recognizes the gp33 peptide on H-2K^b. We cultured P14 TCR transgenic T cells with gp33 peptide and irradiated splenocytes from mice lacking αβT cells (*TCRα*$^{-/-}$) and assessed phospho-PD-1 after 72 hours. WT T cells all expressed cell surface PD-1 and had significantly higher phospho-PD-1 staining than background staining detected in *Pdcd1*$^{-/-}$ T cells (**Fig. 2F**). This indicates that the phospho-PD-1 mAb is sensitive enough to detect PD-1 signaling in primary mouse T cells in response to PD-1 ligands on APCs.

Detection of PD-1 signaling in mouse TILs

We next examined whether the phospho-PD-1 mAb could detect PD-1 signaling in an *in vivo* setting. We examined two tumor models: MC38 colorectal adenocarcinoma and BRAF.PTEN melanoma, both of which express PD-L1 (44). CD8$^+$ TILs expressing cell surface PD-1 (from MC38 tumors) had detectable phospho-PD-1 (**Fig. 3A**). CD8$^+$ TILs from a *Pdcd1*-deficient mouse had no detectable phospho-PD-1 signal, demonstrating the specificity of the phospho-PD-1 mAb (**Fig. 3A**). In mice with either MC38 or BRAF.PTEN tumors, CD8$^+$ TILs and CD8$^+$ T cells from the dLNs that expressed PD-1 had significantly higher phospho-PD-1 signal than PD-1$^-$CD8$^+$ T cells (**Fig. 3B**). There was a similar level of phospho-PD-1 signal in PD-1$^+$ T cells from MC38 and BRAF.PTEN tumors.

We chose the MC38 colorectal adenocarcinoma tumor model for further studies because the TILs in this model express high PD-1 and have been shown to be suppressed directly by PD-L1 on MC38 tumor cells (44). The percentage of CD8$^+$ TILs that expressed PD-1 increased during tumor progression and plateaued at day 10 (**Fig. 3C**). This occurred concurrently with a progressive decrease in the percentage of CD8$^+$ T cells expressing granzyme B, a marker of CD8$^+$ effector T cells (**Fig. 3C**).

Published OnlineFirst October 11, 2021; DOI: 10.1158/2326-6066.CIR-21-0493

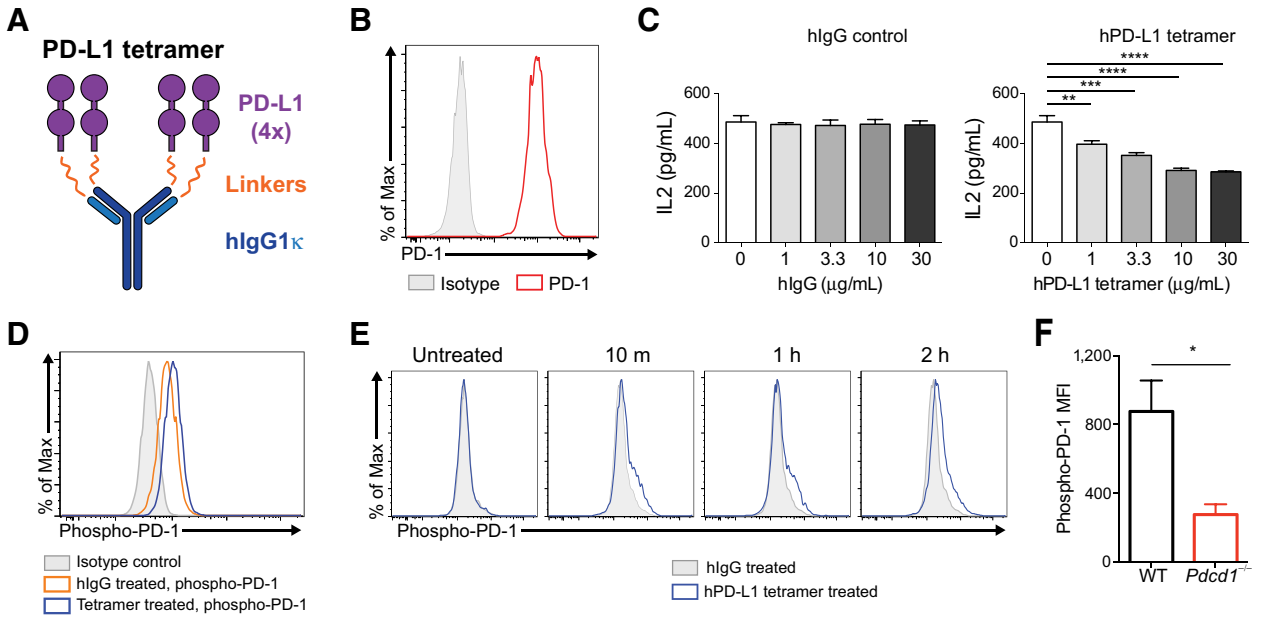

Figure 2.

Detection of PD-1 ligation *in vitro*. **A,** Schematic of mPD-L1-Kappa/mPD-L1-hIgG1 fusion protein (PD-L1 tetramer). **B,** Cell surface expression of hPD-1 in Jurkat hPD-1 cells without treatment. **C,** IL2 secretion at 24 hours following culture of Jurkat-hPD-1 cells with PD-L1 tetramer or hIgG control antibody with concurrent stimulation by anti-CD3 and anti-CD28. **D,** Phospho-PD-1 expression in Jurkat-hPD-1 cells treated with PD-L1 tetramer or hIgG control for 24 hours after stimulation with anti-CD3 and anti-CD28. **E,** Time course of phospho-PD-1 expression in Jurkat-hPD-1 cells cultured with PD-L1 tetramer or hIgG control after 24-hour stimulation with anti-CD3 and anti-CD28. h, hour(s); m, minutes. **F,** Phospho-PD-1 signal in mouse WT versus *Pdcd1*$^{-/-}$ P14 TCR Tg T cells cultured with splenocytes and gp33 peptide for 72 hours. MFI, mean fluorescence intensity. All data shown are representative of at least two independent experiments. For **C**, one-way ANOVA was used to compare without hPD-L1 tetramer treatment (0 μg/mL) to the groups with hPD-L1 tetramer treatment (1 μg/mL, 3.3 μg/mL, 10 μg/mL, and 30 μg/mL, respectively). For **F**, two-tailed unpaired *t* test was used to compare WT and *Pdcd1*$^{-/-}$ groups). *P* value <0.05 (*), <0.01 (**), <0.001 (***), <0.0001 (****). Standard deviation of the mean (SD) is shown.

We next implanted WT and *Pdcd1*$^{-/-}$ mice with 1×10^5 MC38 tumor cells, a dose which grows progressively in WT mice but is cleared by the majority of *Pdcd1*$^{-/-}$ mice (44). At days 7, 10, and 20 of tumor growth, we isolated lymphocytes from tumors and dLNs and analyzed the expression of phospho-PD-1. The phospho-PD-1 signal was strongest in CD8$^+$PD-1$^+$ TILs (**Fig. 3D**) and was lower, but readily detectable, in CD8$^+$PD-1$^+$ T cells from the dLNs (**Fig. 3E**). This pattern of phospho-PD-1 expression could not be attributed to the larger size of activated cells, as this pattern was absent in cells stained with isotype control antibody (**Fig. 3A**). The specificity of the phospho-PD-1 mAb staining was confirmed by the absence of phospho-PD-1 expression in *Pdcd1*$^{-/-}$ T cells.

We also assessed the level of phospho-PD-1 signaling in Tregs in the dLNs and tumors at day 10 of MC38 tumor growth (**Fig. 3F** and **G**). To identify Tregs, we used the GFP expression in transgenic *Foxp3*^{GFP} mice. Similar to CD8$^+$ TILs, PD-1$^+$ Tregs from both dLNs and tumors expressed a detectable phospho-PD-1 signal, whereas PD-1$^-$ Tregs did not express phospho-PD-1 (**Fig. 3F** and **G**). These results show that the phospho-PD-1 mAb can be used to specifically assess PD-1 signaling in different intratumoral T-cell subsets.

PD-1$^+$ TILs coexpressing TIM-3 expressed higher phospho-PD-1

To test the hypothesis that not all PD-1$^+$ TILs had equivalent levels of phospho-PD-1 signaling, we isolated TILs from MC38 tumors late during tumor growth (day 20) and compared phospho-PD-1 in T cells that expressed TIM-3, PD-1, or both (**Fig. 4A** and **B**). A substantial fraction of PD-1$^+$CD8$^+$ TILs also expressed TIM-3, and these T cells have been shown to be more dysfunctional than PD-1$^+$CD8$^+$ T cells that do not express TIM-3 (45–47). There were almost no PD-1$^-$ TILs that expressed TIM-3 (**Fig. 4A**). We detected phospho-PD-1 in CD8$^+$ TILs that expressed PD-1 regardless of TIM-3 expression. However, PD-1$^+$TIM-3$^+$ TILs had a higher mean fluorescence intensity (MFI) of phospho-PD-1 compared to PD-1$^+$TIM-3$^-$ TILs (**Fig. 4B** and **C**). Similarly, PD-1$^+$TIM-3$^+$ Tregs expressed higher phospho-PD-1 (**Fig. 4D**). Together, these data indicate that CD8$^+$ T cells are more dysfunctional, as marked by the coexpression of PD-1 and TIM-3, and exhibit higher PD-1 signaling as evidenced by higher phospho-PD-1.

PD-1 blockade decreased PD-1 phosphorylation in mouse TILs

To test the hypothesis that PD-1 blockade would result in diminished phospho-PD-1 signaling in TILs, we administered PD-1 blocking mAb to MC38 tumor–bearing mice and evaluated phospho-PD-1 expression in T cells from tumors and dLNs one day after the third treatment (day 14). Following PD-1 antibody treatment, there was a decrease in the phospho-PD-1 signal in CD8$^+$ T cells in tumors but no difference in the dLNs (**Fig. 4E**). The decrease in phospho-PD-1 was more evident in PD-1$^+$TIM-3$^+$ TILs (**Fig. 4E**). In contrast to CD8$^+$ T cells, PD-1 blockade did not reduce phospho-PD-1 in total Tregs or TIM-3$^+$ Tregs (**Fig. 4F**).

Phospho-PD-1 signal in human T cells

To test phospho-PD-1 detection in primary human T cells, we stimulated purified human CD3$^+$ T cells with anti-CD3 and anti-CD28 to induce PD-1 expression (**Fig. 5A**) and subsequently treated these cells with PD-L1 tetramer or control. Treatment with PD-L1 tetramer led to an increase in phospho-PD-1 signal in both CD4$^+$ and CD8$^+$ human T cells (**Fig. 5A–C**). Anti-CD3/28

Published OnlineFirst October 11, 2021; DOI: 10.1158/2326-6066.CIR-21-0493

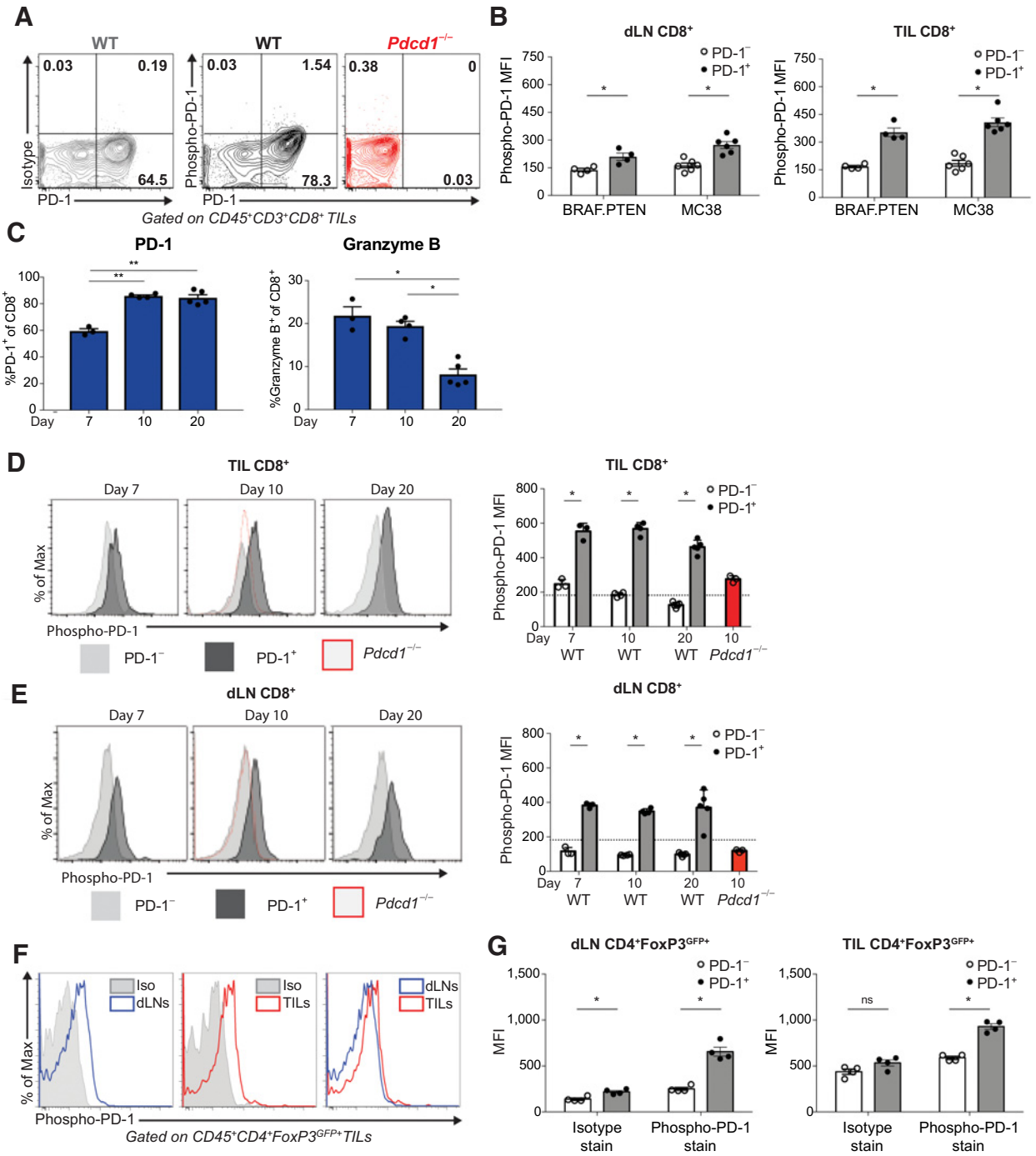

Figure 3.

PD-1 signaling in T cells from tumor-bearing mice. 1×10^5 MC38 tumor cells were implanted s.c. into mice on day 0. Immune cells were isolated from tumors and dLNs at the indicated time points. **A,** $CD8^+$ TILs from WT mice (center) or *Pdcd1*$^{-/-}$ mice (right) were evaluated for expression of cell surface PD-1 and phosphorylated PD-1. $CD8^+$ TILs from WT mice were also stained with isotype control antibody (left). **B,** Phospho-PD-1 in PD-1$^+$ and PD-1$^-$ $CD8^+$ T cells from the dLNs and tumors of WT mice bearing BRAF.PTEN or MC38 tumors. MFI, mean fluorescence intensity. **C,** Percentage of $CD8^+$ T cells expressing PD-1 or granzyme B in TILs from WT mice with MC38 tumors on days 7, 10, and 20. **D** and **E,** MFI of phospho-PD-1 in PD-1$^+$ and PD-1$^-$ $CD8^+$ T cells from tumors (**D**) and dLNs (**E**) of WT mice on days 7, 10, and 20. $CD8^+$ T cells from *Pdcd1*$^{-/-}$ mice also were evaluated on day 10 after implantation with MC38 tumor cells. Dotted line shows level of isotype control stain on $CD8^+$PD-1$^+$ T cells from tumors of WT mice. **F,** $CD4^+FoxP3^{GFP+}$ Tregs from dLNs (left) or tumors (middle) from WT mice with MC38 tumors were evaluated on day 20 for intracellular phospho-PD-1 and compared to isotype control (Iso). Comparison of phospho-PD-1 in Tregs from tumors versus dLNs (right). **G,** Phospho-PD-1 in PD-1$^+$ and PD-1$^-$ Tregs from dLNs (left) or tumors (right) of WT mice with MC38 tumors on day 20. All data shown are representative of at least two independent experiments ($n \geq 4$ mice per group). For **B**, **D**, and **F**, two-tailed unpaired *t* test was used to compare MFI between two groups. For **C**, one-way ANOVA was used to compare one group with the two other groups. *P* value <0.05 (*), <0.01 (**), ns, not significant. SD is shown.

Published OnlineFirst October 11, 2021; DOI: 10.1158/2326-6066.CIR-21-0493

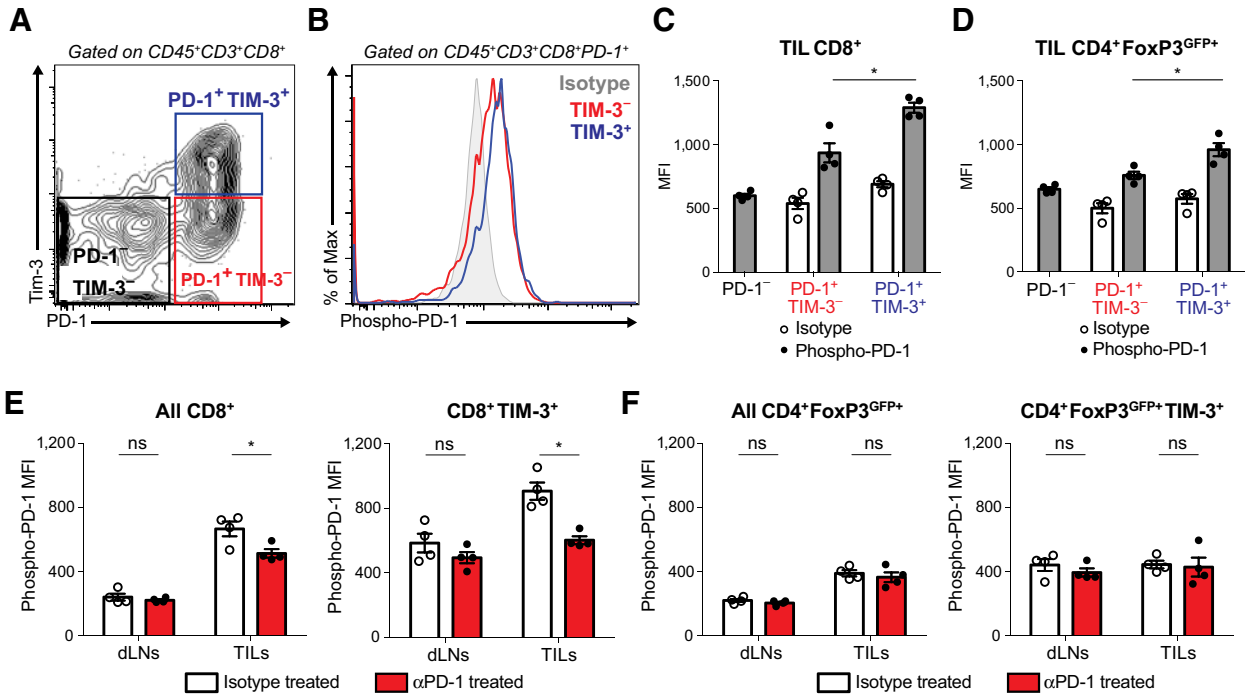

Figure 4.

PD-1 blockade reduces PD-1 signaling in T cells from tumor-bearing mice. 1×10^5 MC38 tumor cells were implanted s.c. into WT mice on day 0. Immune cells were isolated from tumors and dLNs. **A,** $CD8^+$ TILs from WT mice were evaluated for surface expression of PD-1 and TIM-3 on day 20. **B,** Phospho-PD-1 in $TIM\text{-}3^-$ versus $TIM\text{-}3^+$ $PD\text{-}1^+$ TILs were compared. **C** and **D,** Quantification of phospho-PD-1 in $PD\text{-}1^-$ versus $PD\text{-}1^+$ $TIM\text{-}3^-$ versus $PD\text{-}1^+$ $TIM\text{-}3^+$ $CD8^+$ and Treg TILs. **E** and **F,** PD-1 blocking antibody (200 μg, 1A12) or isotype control was administered on days 7, 10, and 13, and T cells from tumors and dLNs were assayed for phospho-PD-1 expression on day 14. MFI of phospho-PD-1 from all $CD8^+$ T cells (left) and $PD\text{-}1^+$ $TIM\text{-}3^+$ $CD8^+$ T cells (right; **E**), as well as all $CD4^+FoxP3\text{-}GFP^+$ T cells (left) and $PD\text{-}1^+$ $TIM\text{-}3^+$ $CD4^+FoxP3\text{-}GFP^+$ T cells (right; **F**) are shown. All data shown are representative of at least two independent experiments ($n \geq 4$ mice per group). For **C**–**F**, two-tailed unpaired *t* test was used to compare MFI between two groups. *P* value <0.05 (*), ns, not significant ($P > 0.05$). SD is shown.

stimulation also induces PD-L1 expression on T cells (48), which may account for the phospho-PD-1 signal in control Ig–treated cells. Thus, the phospho-PD-1 mAb was able to detect PD-1 signaling in primary human T cells.

Because PD-1 blockade reduced PD-1 signaling in mouse tumor models (**Fig. 4E**), we tested whether we could observe changes in phospho-PD-1 in T cells from the peripheral blood of patients with Hodgkin lymphoma following treatment with a combination of an anti–PD-1 and an investigational anti–LAG-3. We found that following treatment, phospho-PD-1 decreased in both $CD4^+$ T cells and $CD8^+$ T cells (**Fig. 5D** and **F**), as well as in $CD45RO^+CCR7^+$ (central memory) $CD4^+$ and $CD8^+$ T cells (**Fig. 5E** and **F**).

Discussion

PD-1 is expressed on the surface of T cells following activation, but inhibitory signals are not transmitted into the cells unless PD-1 is ligated by PD-L1 or PD-L2 (19). Therefore, it is challenging to study PD-1 activity and response to therapeutic blocking antibodies due to the inability to distinguish $PD\text{-}1^+$ cells receiving a PD-1 ligand signal from those that are not receiving a signal. Currently, there exists no tool that can directly detect PD-1 signaling in lymphocytes either *in vitro* or *in vivo*. We developed a mAb that can specifically detect PD-1 signaling. Because phosphorylation of Y248 of the ITSM motif of human and mouse PD-1 is essential for the initiation of inhibitory signals, we reasoned that an antibody recognizing the phosphorylated PD-1 ITSM would provide a means of detecting PD-1 signaling. *Pdcd1*-deficient mice were immunized with a peptide immunogen encompassing the ITSM motif and phosphorylated Y248 residue. Eight amino acids of this sequence are identical in human and mouse PD-1. The phospho-PD-1 mAb was validated by Western blot using protein extracts from pervanadate-treated human and mouse T cells. The ability of the phospho-PD-1 mAb to detect phosphorylation of PD-1 by flow cytometry was confirmed in Jurkat-hPD-1 T cells. Thus, we conclude that our phospho-PD-1 mAb is capable of detecting the phosphorylated form of the PD-1 ITSM by both Western blot and flow cytometry.

We showed the phospho-PD-1 mAb could detect PD-1 ITSM phosphorylation following PD-1 ligation by PD-L1. To this end, a PD-L1 tetramer was employed to ligate PD-1 on Jurkat-hPD-1 cells, as well as human $CD4^+$ and $CD8^+$ T cells. The results of our experiments indicate that the phospho-PD-1 mAb can be used to detect active PD-1 inhibitory signals triggered by PD-L1 ligation. Our studies also show that the phospho-PD-1 mAb is sensitive enough to be used for primary mouse T cells to detect a phospho-PD-1 signal delivered by PD-1 ligands on APCs. The specificity of the phospho-PD-1 antibody for PD-1 phosphorylation, and no other phosphorylated proteins, was validated by the absence of phospho-PD-1 expression in activated $Pdcd1^{-/-}$ T cells by flow cytometry. Another study reports a rabbit polyclonal antibody that can detect phospho-PD-1, but this is a finite resource (49).

Our studies revealed that the phospho-PD-1 antibody can detect PD-1 signaling in T cells from tumors and dLNs in the *in vivo* MC38 mouse tumor model. We hypothesized that not all $PD\text{-}1^+$ TILs have

Published OnlineFirst October 11, 2021; DOI: 10.1158/2326-6066.CIR-21-0493

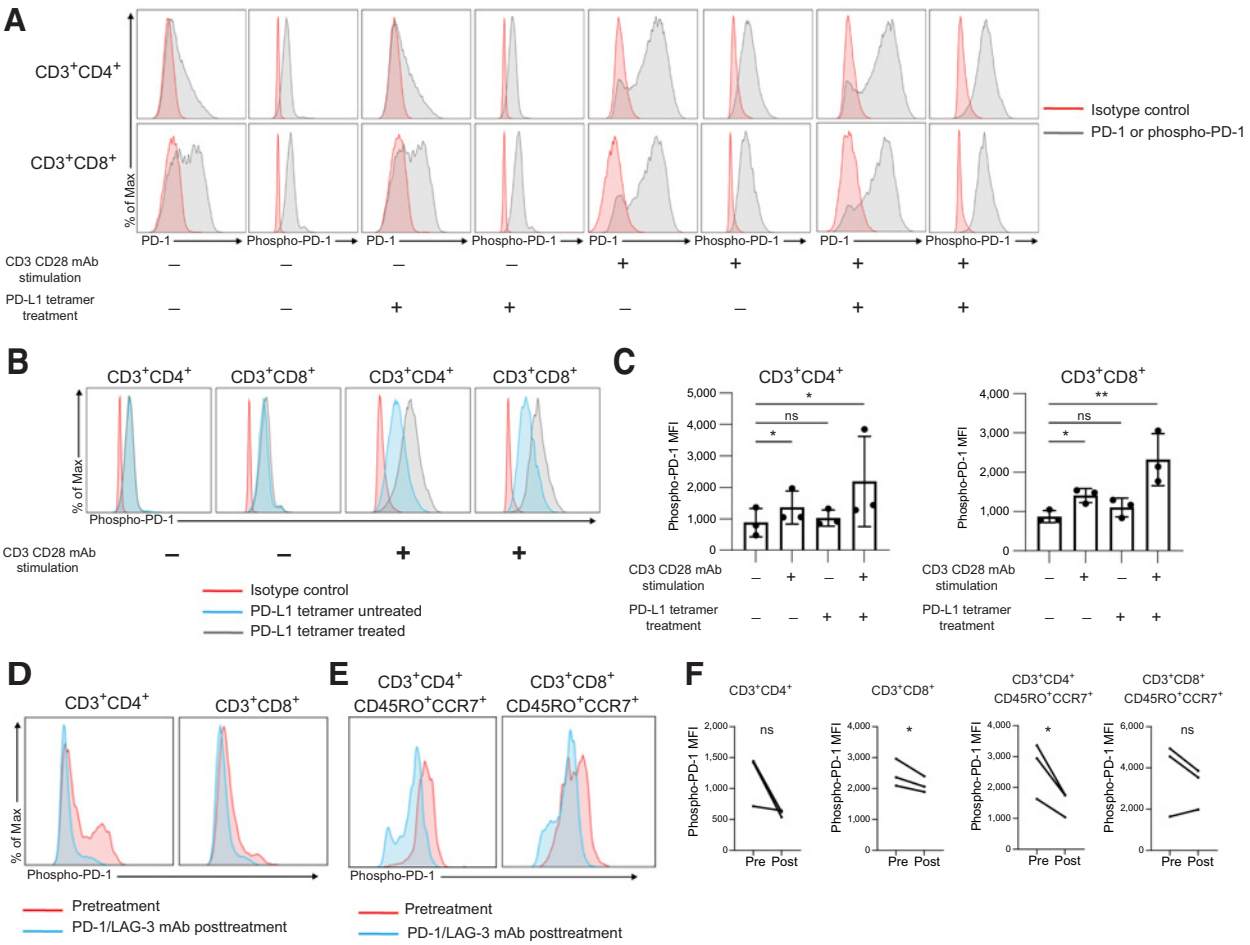

Figure 5.

Phosphorylation of PD-1 in human CD4$^+$ and CD8$^+$ T cells from healthy donors and PD-1 plus LAG-3–treated Hodgkin lymphoma patients. **A–C,** Human CD3$^+$ T cells from healthy donors were isolated and cultured in 24-well plates with or without CD3 and CD28 mAb stimulation as indicated. After 24 hours, PD-L1 tetramer was added to the indicated wells and expression of PD-1 and phospho-PD-1 was analyzed by flow cytometry 24 hours later. Red represents isotype control antibody; gray represents the indicated PD-1 or phospho-PD-1 antibody. **A,** Histograms from one donor; representative of three healthy donors. **B,** Overlay of histograms from **A** of phospho-PD-1 expression with and without PD-L1 tetramer treatment. **C,** MFI of phospho-PD-1 expression. $n = 3$; *, $P < 0.05$, paired t test. **D–F,** Expression of phospho-PD-1 in CD3$^+$CD4$^+$ and CD3$^+$CD8$^+$ T cells (**D**) and CD3$^+$CD4$^+$CD45RO$^+$CCR7$^+$ or CD3$^+$CD8$^+$CD45RO$^+$CCR7$^+$ central memory T cells (**E**) from Hodgkin lymphoma patients before and after treatment with PD-1 and LAG-3 mAbs. **F,** MFI of pretreatment and posttreatment samples from **D** and **E**. $n = 3$; *, $P < 0.05$, paired t test. Connected points indicate paired samples.

the same level of phospho-PD-1 signaling. T cells that express multiple coinhibitory molecules are more dysfunctional than T cells that express one or none (27). For example, TILs that coexpress PD-1 and TIM-3 produce fewer cytokines than T cells that only express PD-1 (28). This could be due, in part, to enhanced PD-1 signaling in TIM-3$^+$ cells. Our results demonstrated that more dysfunctional T cells, such as PD-1$^+$TIM-3$^+$ TILs, have higher levels of PD-1 signaling, as measured by our phospho-PD-1 antibody.

MC38 tumors are responsive to PD-1 blockade, presumably because PD-1 blockade reduces the immunoinhibitory activity of the PD-1 pathway (50). We showed PD-1 blockade led to reduced phospho-PD-1 in CD8$^+$ TILs from MC38 tumors. Because PD-1$^+$TIM-3$^+$ TILs from untreated tumors had higher phospho-PD-1 compared to PD-1$^+$TIM-3$^-$ TILs, we predicted that PD-1 blockade would reduce phospho-PD-1 to a greater extent in the PD-1$^+$TIM-3$^+$ TILs. Indeed, following PD-1 mAb treatment, the decrease in phospho-PD-1 was much more striking in PD-1$^+$TIM-3$^+$ CD8$^+$ T cells compared to PD-1$^+$TIM-3$^-$ CD8$^+$ T cells. PD-1 mAb treatment did not lead to any change of phospho-PD-1 in Tregs or TIM-3$^+$ Tregs from either tumors or dLNs. These results suggest phospho-PD-1 in CD8$^+$ T cells could be used to follow the response to PD-1 blockade in patients. We analyzed phospho-PD-1 in T cells from the peripheral blood of patients with Hodgkin lymphoma before and after combination treatment with PD-1 and LAG-3 mAbs (nivolumab and relatlimab). The levels of phospho-PD-1 were reduced in total CD4$^+$ and CD8$^+$ T cells, as well as central memory CD4$^+$ and CD8$^+$ T cells. Notably, CD4 $^+$T cells are required for clinical responses to PD-1 ICB (51) These results support further study of phospho-PD-1 as a biomarker of response to ICB.

Taken together, these data indicate that phosphorylation of the PD-1 ITSM in the intracellular tail can be used as a measure of active PD-1 signaling and thus of response to PD-1 ICB. We showed that phospho-PD-1 in CD8$^+$ TILs was reduced following PD-1 blockade in a PD-1 sensitive tumor model. TILs that coexpressed

multiple coinhibitory molecules had higher levels of phospho-PD-1 than cells that expressed one or none, and anti–PD-1 therapy diminished this PD-1 signaling. These results show that the phospho-PD-1 mAb is a valuable tool for studying PD-1 biology. Phospho-PD-1 mAb may have other utilities, such as evaluating antibody or small molecule agonists of the PD-1 pathway, which could be employed to induce immune tolerance or alleviate autoimmunity. Additional studies with large patient cohorts are needed to determine whether the level of phospho-PD-1 expression may accurately serve as a biomarker for responsiveness to PD-1 blockade or combination therapy.

Authors' Disclosures

X. Bu reports a patent for anti-phosphotyrosinylated PD-1 antibodies and uses thereof pending. V.R. Juneja reports grants from National Science Foundation and NDSEG during the conduct of the study; patent US20200115452A1 pending; and is an employee of BioNTech US. K.M. Mahoney reports grants from Bristol Myers Squibb outside the submitted work. E.A. Greenfield reports a patent for methods related to TIM3, a Th1-specific cell surface molecule, for activating antigen presenting cells issued and with royalties paid. P. Armand reports other support from Bristol Myers Squibb during the conduct of the study, as well as other support (consultancy) from Merck, BMS, Pfizer, Affimed, Adaptive, Infinity, ADC Therapeutics, Celgene, Morphosys, Daiichi Sankyo, Miltenyi, Tessa, GenMab, C4, Enterome, Regeneron, Epizyme, AstraZeneca, and Genentech, other support (institutional research funding) from Merck, Bristol Myers Squibb, Affimed, Adaptive, Roche, Tensha, Otsuka, Sigma Tau, Genentech, IGM, and Kite, and other support (speaker honoraria) from Merck and Bristol Myers Squibb outside the submitted work. J. Ritz reports grants from NIH during the conduct of the study, as well as grants from Amgen, Equillium, and Kite/Gilead and personal fees from Akron Biotech, Avribio, Clade Therapeutics, Garuda Therapeutics, Immunitas Therapeutics, LifeVault Bio, Novartis, Rheos Medicines, Talaris Therapeutics, and TScan Therapeutics outside the submitted work. A.H. Sharpe reports grants from NIH (P01 AI56299 and P50 CA101942) during the conduct of the study; personal fees from Surface Oncology, Sqz Biotech, Selecta, Elstar, and Elpiscience, other support from Monopteros, and grants from Novartis, Merck, Roche, Ipsen, UCB, Quark Ventures/Iome, and Bicara outside the submitted work; patent 7,432,059 with royalties paid from Roche, Merck, Bristol Myers Squibb, EMD Serono, Boehringer Ingelheim, AstraZeneca, Leica, Mayo Clinic, Dako, and Novartis, patent 7,722,868 with royalties paid from Roche, Merck, Bristol Myers Squibb, EMD Serono, Boehringer Ingelheim, AstraZeneca, Leica, Mayo Clinic, Dako, and Novartis, patent 8,652,465 licensed to Roche, patent 9,457,080 licensed to Roche, patent 9,683,048 licensed to Roche, patent 9,815,898 licensed to Novartis, patent 9,845,356 licensed to Novartis, patent 10,202,454 licensed to Novartis, patent 10,457,733 licensed to Novartis, patent 9,580,684 issued, patent 9,988,452 issued, and patent 10,370,446 issued; and is on the scientific advisory boards for the Massachusetts General Cancer Center, Program in Cellular and Molecular Medicine at Boston Children's Hospital, the Human Oncology and Pathogenesis Program at Memorial Sloan Kettering Cancer Center, and the GlaxoSmithKine Oncology Executive Advisory Board and Janssen Immunology Advisory Board. G.J. Freeman reports grants from NIH and NCI during the conduct of the study; personal fees from Roche, Bristol Myers Squibb, Xios, Origimed, Triursus, iTeos, NextPoint, IgM, Jubilant, Trillium, GV20, and Geode outside the submitted work; and a patent for PD-1/PD-L1 pathway issued, licensed, and with royalties paid from Roche, a patent for PD-1/PD-L1 pathway issued, licensed, and with royalties paid from Merck MSD, a patent for PD-1/PD-L1 pathway issued, licensed, and with royalties paid from Bristol Myers Squibb, a patent for PD-1/PD-L1 pathway issued, licensed, and with royalties paid from Merck KGA, a patent for PD-1/PD-L1 pathway issued, licensed, and with royalties paid from Eli Lilly, a patent for PD-1/PD-L1 pathway issued, licensed, and with royalties paid from Boehringer Ingelheim, a patent for PD-1/PD-L1 pathway issued, licensed, and with royalties paid from AstraZeneca, a patent for PD-1/PD-L1 pathway issued, licensed, and with royalties paid from Dako, a patent for PD-1/PD-L1 pathway issued, licensed, and with royalties paid from Leica, a patent for PD-1/PD-L1 pathway issued, licensed, and with royalties paid from Mayo Clinic, and a patent for PD-1/PD-L1 and TIM-3 pathways issued, licensed, and with royalties paid from Novartis. No disclosures were reported by the other authors.

Authors' Contributions

X. Bu: Conceptualization, investigation, methodology, writing–original draft, writing–review and editing. **V.R. Juneja:** Conceptualization, investigation, methodology, writing–original draft, writing–review and editing. **C.G. Reynolds:** Investigation, writing–review and editing. **K.M. Mahoney:** Investigation, writing–review and editing. **M.T. Bu:** Investigation, writing–review and editing. **K.A. McGuire:** Investigation, writing–review and editing. **S. Maleri:** Investigation, writing–review and editing. **P. Hua:** Investigation, writing–review and editing. **B. Zhu:** Investigation, writing–review and editing. **S.R. Klein:** Investigation, writing–review and editing. **E.A. Greenfield:** Investigation, writing–review and editing. **P. Armand:** Conceptualization, resources, supervision, investigation, writing–review and editing. **J. Ritz:** Conceptualization, resources, supervision, investigation, writing–review and editing. **A.H. Sharpe:** Conceptualization, resources, supervision, funding acquisition, writing–original draft, writing–review and editing. **G.J. Freeman:** Conceptualization, resources, supervision, funding acquisition, investigation, writing–original draft, writing–review and editing.

Acknowledgments

The authors thank Peter Sage for helpful discussions and Kristin McHugh and Mikaela McDonough for their help in collecting clinical samples.

This work was supported by grants from the NIH (P01 AI56299 and P50 CA101942 to A.H. Sharpe and G.J. Freeman and P50 CA206963 to G.J. Freeman). V.R. Juneja was funded by graduate fellowships from the National Science Foundation and the Department of Defense. K.A. McGuire was funded by the Irvington Postdoctoral Fellowship from the Cancer Research Institute. K.M. Mahoney was funded by the Claudia Adams Barr Program for Innovative Cancer Research; the 2014 AACR Anna D. Barker Fellowship in Basic Cancer Research, Grant Number 14-40-01-MAHO; and the ASCO Young Investigator Award supported by Kidney Cancer Association.

The costs of publication of this article were defrayed in part by the payment of page charges. This article must therefore be hereby marked *advertisement* in accordance with 18 U.S.C. Section 1734 solely to indicate this fact.

Received June 21, 2021; revised August 30, 2021; accepted October 8, 2021; published first October 11, 2021.

References

1. Mahoney KM, Rennert PD, Freeman GJ. Combination cancer immunotherapy and new immunomodulatory targets. Nat Rev Drug Discov 2015;14:561–84.
2. Zou W, Wolchok JD, Chen L. PD-L1 (B7-H1) and PD-1 pathway blockade for cancer therapy: mechanisms, response biomarkers, and combinations. Sci Transl Med 2016;8:328rv4.
3. Chamoto K, Hatae R, Honjo T. Current issues and perspectives in PD-1 blockade cancer immunotherapy. Int J Clin Oncol 2020;25:790–800.
4. Postow MA, Callahan MK, Wolchok JD. Immune checkpoint blockade in cancer therapy. J Clin Oncol 2015;33:1974–82.
5. Blons H, Garinet S, Laurent-Puig P, Oudart JB. Molecular markers and prediction of response to immunotherapy in non-small cell lung cancer, an update. J Thorac Dis 2019;11:S25–36.
6. Berger KN, Pu JJ. PD-1 pathway and its clinical application: a 20 year journey after discovery of the complete human PD-1 gene. Gene 2018;638:20–5.
7. Herbst RS, Soria JC, Kowanetz M, Fine GD, Hamid O, Gordon MS, et al. Predictive correlates of response to the anti-PD-L1 antibody MPDL3280A in cancer patients. Nature 2014;515:563–7.
8. Lagos GG, Izar B, Rizvi NA. Beyond tumor PD-L1: emerging genomic biomarkers for checkpoint inhibitor immunotherapy. Am Soc Clin Oncol Educ Book 2020;40:1–11.
9. Taube JM, Klein A, Brahmer JR, Xu H, Pan X, Kim JH, et al. Association of PD-1, PD-1 ligands, and other features of the tumor immune microenvironment with response to anti-PD-1 therapy. Clin Cancer Res 2014;20:5064–74.
10. Francisco LM, Sage PT, Sharpe AH. The PD-1 pathway in tolerance and autoimmunity. Immunol Rev 2010;236:219–42.
11. Wei F, Zhong S, Ma Z, Kong H, Medvec A, Ahmed R, et al. Strength of PD-1 signaling differentially affects T-cell effector functions. Proc Natl Acad Sci U S A 2013;110:E2480–9.

12. Bellucci R, Martin A, Bommarito D, Wang K, Hansen SH, Freeman GJ, et al. Interferon-gamma-induced activation of JAK1 and JAK2 suppresses tumor cell susceptibility to NK cells through upregulation of PD-L1 expression. Oncoimmunology 2015;4:e1008824.
13. Hsu J, Hodgins JJ, Marathe M, Nicolai CJ, Bourgeois-Daigneault MC, Trevino TN, et al. Contribution of NK cells to immunotherapy mediated by PD-1/PD-L1 blockade. J Clin Invest 2018;128:4654–68.
14. Tan CL, Kuchroo JR, Sage PT, Liang D, Francisco LM, Buck J, et al. PD-1 restraint of regulatory T cell suppressive activity is critical for immune tolerance. J Exp Med 2021;218:e20182232.
15. Kumagai S, Togashi Y, Kamada T, Sugiyama E, Nishinakamura H, Takeuchi Y, et al. The PD-1 expression balance between effector and regulatory T cells predicts the clinical efficacy of PD-1 blockade therapies. Nat Immunol 2020;21:1346–58.
16. Gordon SR, Maute RL, Dulken BW, Hutter G, George BM, McCracken MN, et al. PD-1 expression by tumour-associated macrophages inhibits phagocytosis and tumour immunity. Nature 2017;545:495–9.
17. Baumeister SH, Freeman GJ, Dranoff G, Sharpe AH. Coinhibitory pathways in immunotherapy for cancer. Annu Rev Immunol 2016;34:539–73.
18. Riley JL. PD-1 signaling in primary T cells. Immunol Rev 2009;229:114–25.
19. Chemnitz JM, Parry RV, Nichols KE, June CH, Riley JL. SHP-1 and SHP-2 associate with immunoreceptor tyrosine-based switch motif of programmed death 1 upon primary human T cell stimulation, but only receptor ligation prevents T cell activation. J Immunol 2004;173:945–54.
20. Okazaki T, Maeda A, Nishimura H, Kurosaki T, Honjo T. PD-1 immunoreceptor inhibits B cell receptor-mediated signaling by recruiting src homology 2-domain-containing tyrosine phosphatase 2 to phosphotyrosine. Proc Natl Acad Sci U S A 2001;98:13866–71.
21. Yokosuka T, Takamatsu M, Kobayashi-Imanishi W, Hashimoto-Tane A, Azuma M, Saito T. Programmed cell death 1 forms negative costimulatory microclusters that directly inhibit T cell receptor signaling by recruiting phosphatase SHP2. J Exp Med 2012;209:1201–17.
22. Keir ME, Francisco LM, Sharpe AH. PD-1 and its ligands in T-cell immunity. Curr Opin Immunol 2007;19:309–14.
23. Hui E, Cheung J, Zhu J, Su X, Taylor MJ, Wallweber HA, et al. T cell costimulatory receptor CD28 is a primary target for PD-1-mediated inhibition. Science 2017;355:1428–33.
24. Patsoukis N, Duke-Cohan JS, Chaudhri A, Aksoylar HI, Wang Q, Council A, et al. Interaction of SHP-2 SH2 domains with PD-1 ITSM induces PD-1 dimerization and SHP-2 activation. Commun Biol 2020;3:128.
25. Latchman Y, Wood CR, Chernova T, Chaudhary D, Borde M, Chernova I, et al. PD-L2 is a second ligand for PD-1 and inhibits T cell activation. Nat Immunol 2001;2:261–8.
26. Mizuno R, Sugiura D, Shimizu K, Maruhashi T, Watada M, Okazaki IM, et al. PD-1 primarily targets TCR signal in the inhibition of functional T cell activation. Front Immunol 2019;10:630.
27. Blackburn SD, Shin H, Haining WN, Zou T, Workman CJ, Polley A, et al. Coregulation of CD8+ T cell exhaustion by multiple inhibitory receptors during chronic viral infection. Nat Immunol 2009;10:29–37.
28. Sakuishi K, Apetoh L, Sullivan JM, Blazar BR, Kuchroo VK, Anderson AC. Targeting Tim-3 and PD-1 pathways to reverse T cell exhaustion and restore anti-tumor immunity. J Exp Med 2010;207:2187–94.
29. Cooper ZA, Juneja VR, Sage PT, Frederick DT, Piris A, Mitra D, et al. Response to BRAF inhibition in melanoma is enhanced when combined with immune checkpoint blockade. Cancer Immunol Res 2014;2:643–54.
30. Quigley M, Pereyra F, Nilsson B, Porichis F, Fonseca C, Eichbaum Q, et al. Transcriptional analysis of HIV-specific CD8+ T cells shows that PD-1 inhibits T cell function by upregulating BATF. Nat Med 2010;16:1147–51.
31. Chaudhri A, Xiao Y, Klee AN, Wang X, Zhu B, Freeman GJ. PD-L1 binds to B7-1 only in Cis on the same cell surface. Cancer Immunol Res 2018;6:921–9.
32. Keir ME, Freeman GJ, Sharpe AH. PD-1 regulates self-reactive CD8+ T cell responses to antigen in lymph nodes and tissues. J Immunol 2007;179:5064–70.
33. Pircher H, Burki K, Lang R, Hengartner H, Zinkernagel RM. Tolerance induction in double specific T-cell receptor transgenic mice varies with antigen. Nature 1989;342:559–61.
34. Kohler G, Milstein C. Continuous cultures of fused cells secreting antibody of predefined specificity. Nature 1975;256:495–7.
35. Rodig N, Ryan T, Allen JA, Pang H, Grabie N, Chernova T, et al. Endothelial expression of PD-L1 and PD-L2 down-regulates CD8+ T cell activation and cytolysis. Eur J Immunol 2003;33:3117–26.
36. Chemnitz JM, Lanfranco AR, Braunstein I, Riley JL. B and T lymphocyte attenuator-mediated signal transduction provides a potent inhibitory signal to primary human CD4 T cells that can be initiated by multiple phosphotyrosine motifs. J Immunol 2006;176:6603–14.
37. O'Shea JJ, McVicar DW, Bailey TL, Burns C, Smyth MJ. Activation of human peripheral blood T lymphocytes by pharmacological induction of protein-tyrosine phosphorylation. Proc Natl Acad Sci U S A. 1992;89:10306–10.
38. Fantus IG, Kadota S, Deragon G, Foster B, Posner BI. Pervanadate [peroxide(s) of vanadate] mimics insulin action in rat adipocytes via activation of the insulin receptor tyrosine kinase. Biochemistry 1989;28:8864–71.
39. Hsi ED, Siegel JN, Minami Y, Luong ET, Klausner RD, Samelson LE. T cell activation induces rapid tyrosine phosphorylation of a limited number of cellular substrates. J Biol Chem 1989;264:10836–42.
40. Dorfman DM, Brown JA, Shahsafaei A, Freeman GJ. Programmed death-1 (PD-1) is a marker of germinal center-associated T cells and angioimmunoblastic T-cell lymphoma. Am J Surg Pathol 2006;30:802–10.
41. Nakamoto N, Kaplan DE, Coleclough J, Li Y, Valiga ME, Kaminski M, et al. Functional restoration of HCV-specific CD8 T cells by PD-1 blockade is defined by PD-1 expression and compartmentalization. Gastroenterology 2008;134:1927–37, 37 e1–2.
42. Zhu B, Cai G, Hall EO, Freeman GJ. In-fusion assembly: seamless engineering of multidomain fusion proteins, modular vectors, and mutations. Biotechniques 2007;43:354–9.
43. Naito M, Hainz U, Burkhardt UE, Fu B, Ahove D, Stevenson KE, et al. CD40L-Tri, a novel formulation of recombinant human CD40L that effectively activates B cells. Cancer Immunol Immunother 2013;62:347–57.
44. Juneja VR, McGuire KA, Manguso RT, LaFleur MW, Collins N, Haining WN, et al. PD-L1 on tumor cells is sufficient for immune evasion in immunogenic tumors and inhibits CD8 T cell cytotoxicity. J Exp Med 2017;214:895–904.
45. Anderson AC, Joller N, Kuchroo VK. Lag-3, Tim-3, and TIGIT: co-inhibitory receptors with specialized functions in immune regulation. Immunity 2016;44:989–1004.
46. Hashimoto M, Kamphorst AO, Im SJ, Kissick HT, Pillai RN, Ramalingam SS, et al. CD8 T cell exhaustion in chronic infection and cancer: opportunities for interventions. Annu Rev Med 2018;69:301–18.
47. McLane LM, Abdel-Hakeem MS, Wherry EJ. CD8 T cell exhaustion during chronic viral infection and cancer. Annu Rev Immunol 2019;37:457–95.
48. Brown JA, Dorfman DM, Ma FR, Sullivan EL, Munoz O, Wood CR, et al. Blockade of programmed death-1 ligands on dendritic cells enhances T cell activation and cytokine production. J Immunol 2003;170:1257–66.
49. Bardhan K, Aksoylar HI, Le Bourgeois T, Strauss L, Weaver JD, Delcuze B, et al. Phosphorylation of PD-1-Y248 is a marker of PD-1-mediated inhibitory function in human T cells. Sci Rep 2019;9:17252.
50. Woo SR, Turnis ME, Goldberg MV, Bankoti J, Selby M, Nirschl CJ, et al. Immune inhibitory molecules LAG-3 and PD-1 synergistically regulate T-cell function to promote tumoral immune escape. Cancer Res 2012;72:917–27.
51. Zuazo M, Arasanz H, Fernandez-Hinojal G, Garcia-Granda MJ, Gato M, Bocanegra A, et al. Functional systemic CD4 immunity is required for clinical responses to PD-L1/PD-1 blockade therapy. EMBO Mol Med 2019;11:e10293.

AACR American Association for Cancer Research

Cancer Immunology Research

Monitoring PD-1 Phosphorylation to Evaluate PD-1 Signaling during Antitumor Immune Responses

Xia Bu, Vikram R. Juneja, Carol G. Reynolds, et al.

Cancer Immunol Res Published OnlineFirst October 11, 2021.